

# Brain Metabolism of $^{13}\text{N}$ -Ammonia During Acute Hepatic Encephalopathy in Cirrhosis Measured by Positron Emission Tomography

Susanne Keiding,<sup>1,2</sup> Michael Sørensen,<sup>1,2</sup> Dirk Bender,<sup>2</sup> Ole Lajord Munk,<sup>2</sup> Peter Ott,<sup>1</sup> and Hendrik Vilstrup<sup>1</sup>

Animal studies and results from  $^{13}\text{N}$ -ammonia positron emission tomography (PET) in patients with cirrhosis and minimal hepatic encephalopathy suggest that a disturbed brain ammonia metabolism plays a pivotal role in the pathogenesis of hepatic encephalopathy (HE). We studied brain ammonia kinetics in 8 patients with cirrhosis with an acute episode of clinically overt HE (I-IV), 7 patients with cirrhosis without HE, and 5 healthy subjects, using contemporary dynamic  $^{13}\text{N}$ -ammonia PET. Time courses were obtained of  $^{13}\text{N}$ -concentrations in cerebral cortex, basal ganglia, and cerebellum (PET-scans) as well as arterial  $^{13}\text{N}$ -ammonia,  $^{13}\text{N}$ -urea, and  $^{13}\text{N}$ -glutamine concentrations (blood samples) after  $^{13}\text{N}$ -ammonia injection. Regional  $^{13}\text{N}$ -ammonia kinetics was calculated by non-linear fitting of a physiological model of brain ammonia metabolism to the data. Mean permeability–surface area product of  $^{13}\text{N}$ -ammonia transfer across blood–brain barrier in cortex,  $PS_{\text{BBB}}$ , was 0.21 mL blood/min/mL tissue in patients with HE, 0.31 in patients without HE, and 0.34 in healthy controls; similar differences were seen in basal ganglia and cerebellum. Metabolic trapping of blood  $^{13}\text{N}$ -ammonia in the brain showed neither regional, nor patient group differences. Mean net metabolic flux of ammonia from blood into intracellular glutamine in the cortex was 13.4  $\mu\text{mol}/\text{min}/\text{L}$  tissue in patients with cirrhosis with HE, 7.4 in patients without HE, and 2.6 in healthy controls, significantly correlated to blood ammonia. **In conclusion**, increased cerebral trapping of ammonia in patients with cirrhosis with acute HE was primarily attributable to increased blood ammonia and to a minor extent to changed ammonia kinetics in the brain. (HEPATOLOGY 2006;43:42-50.)

The role of ammonia in the pathogenesis of hepatic encephalopathy (HE) and possible deleterious effects on brain energy metabolism and neurotransmission has been extensively studied.<sup>1-4</sup> The effects of experimental porta-caval anastomosis with or without pharmacological manipulations of ammonia metabolism have been examined in rat brain,<sup>5-13</sup> and the effects of

excess ammonia have been tested in astrocyte cell cultures.<sup>14</sup> Human studies of cerebral uptake and metabolism of ammonia included postmortem examinations of brain tissue from patients dying of HE<sup>15</sup> and biochemical analysis of jugular vein blood samples.<sup>16-18</sup> More recently, ammonia metabolism has been tested in positron emission tomography (PET) studies of monkeys,<sup>19</sup> healthy humans,<sup>19-22</sup> and patients with cirrhosis and minimal HE.<sup>20-23</sup> The  $^{13}\text{N}$ -ammonia PET technique can, in conjunction with proper compartmental analysis, give quantitative estimates of kinetic parameters in awake subjects.

Results of early PET studies by Phelps et al.<sup>19</sup> indicated the presence of regional variations in cerebral  $^{13}\text{N}$ -ammonia uptake in normal human subjects. Lockwood et al.<sup>20</sup> subsequently emphasized that the metabolism of ammonia to glutamine in brain influences cerebral ammonia uptake and later calculated a global rate of cerebral  $^{13}\text{N}$ -ammonia metabolism in patients with cirrhosis with minimal HE and healthy controls.<sup>21,22</sup> Recently, Ahl et al.,<sup>23</sup> using dynamic PET studies, found no significant difference of the permeability–surface area product of the trans-

---

Abbreviations: HE, hepatic encephalopathy; PET, positron emission tomography; BBB, blood brain barrier;  $^{13}\text{N}$ -ammonia, sum of  $^{13}\text{N}$ -ammonium ion ( $^{13}\text{NH}_4^+$ ) and  $^{13}\text{N}$ -ammonia free base ( $^{13}\text{NH}_3$ ); CBF, regional cerebral blood flow; PS, permeability surface product; VOI, volume of interest.

From the <sup>1</sup>Department of Medicine V (Hepatology) and <sup>2</sup>PET Center, Aarhus University Hospital, Aarhus, Denmark.

Received March 14, 2005; accepted October 23, 2005.

Supported by grants from the Novo Nordic Foundation and the Danish Medical Research Council (22-02-0337).

Address reprint requests to: Susanne Keiding, M.D., Department of Medicine V, Aarhus University Hospital, Noerrebrogade, 8000 Aarhus C, Denmark. E-mail: susanne@pet.aub.dk; fax: (45) 89-49-30-20.

Copyright © 2005 by the American Association for the Study of Liver Diseases.

Published online in Wiley InterScience (www.interscience.wiley.com).

DOI 10.1002/hep.21001

Potential conflict of interest: Nothing to report.

**Table 1. Clinical Data**

Subjects			Liver Function							HE		
			GEC pt/ref	Pro- thrombin (index)	Albumin ( $\mu\text{mol/L}$ )	Child-Pugh Class	Arterial $\text{pCO}_2$ (kPa)	Arterial Standard $\text{HCO}_3^-$ (mmol/L)	Arterial pH	Arterial Ammonia ( $\mu\text{mol/L}$ )	New Haven Grade	
Cirrhosis with acute HE	8	5/3	60 (50-77)	0.48 (.27-.61)	0.39 (.27-.56)	360 (274-491)	A: 0 B: 1 C: 7	3.91 (3.71-4.27)	23.7 (18.3-27.5)	7.45 (7.38-7.49)	73 (29-97)	I: 1; II:3 III: 2; IV:2
Cirrhosis without HE	7	4/3	54 (47-67)	0.49 (.38-.59)	0.41 (.27-.57)	412 (272-449)	A: 2 B: 0 C: 5	5.35 (4.27-6.62)	27.0 (23.4-28.1)	7.43 (7.38-7.48)	50 (28-78)	no HE
Healthy controls	5	2/3	47 (41-56)	1.0 (.85-1.15)	1.0 (0.83-1.13)	656 (602-726)	—	5.45 (4.83-5.68)	25.2 (24.0-27.1)	7.42 (7.41-7.43)	16 (9-20)	—

NOTE. Patient GEC relative to that for a healthy subject of same age and body weight<sup>49</sup>; Prothrombin index = coagulation factors II + IV + X relative to mean control value. Child-Pugh class<sup>50</sup> and HE grade<sup>24</sup>: number of patients.

Abbreviations: N, number of subjects; M/F, number of males/females; GEC, galactose elimination capacity (mmol/min) pt/ref.

\*Continuous variables are given as mean (range).

fer of  $^{13}\text{N}$ -ammonia across the blood-brain barrier (BBB) between patients with cirrhosis with minimal HE and patients with cirrhosis without HE. No PET studies have been published in patients with cirrhosis with clinically manifest HE. Nevertheless, the previously mentioned studies support a hypothesis that blood-brain transfer of ammonia and the subsequent intracellular metabolism of ammonia are both increased in patients with cirrhosis with HE. To address this issue, we performed dynamic  $^{13}\text{N}$ -ammonia PET studies in brain of patients with cirrhosis with an acute episode of overt HE, patients without HE, and healthy controls. To this end, we made use of the improved spatial and temporal resolution of contemporary PET technology. Kinetic parameters of transfer of  $^{13}\text{N}$ -ammonia (*i.e.*,  $^{13}\text{NH}_3 + ^{13}\text{NH}_4^+$ ) from blood to cells as well as intracellular metabolism of  $^{13}\text{N}$ -ammonia metabolism were estimated separately. Dynamic  $^{13}\text{N}$ -ammonia PET in conjunction with individual measurements of blood contents of  $^{13}\text{N}$ -ammonia and  $^{13}\text{N}$ -metabolites were employed for optimal kinetic modeling of the ammonia metabolism. In addition, regional cerebral blood flow was measured by dynamic  $^{15}\text{O}$ -water scans to obtain parameters of regional cerebral ammonia kinetics based on individual estimates of cerebral  $^{13}\text{N}$ -ammonia clearances and cerebral blood flow.

## Patients and Methods

**Human Subjects.** Eight patients with cirrhosis and an acute episode of clinically overt type C HE, West Haven criteria grades I to IV, Glasgow coma scale score 1 to 12,<sup>24-26</sup> 7 patients with cirrhosis with no recent or previous clinical symptoms of HE, and 5 healthy individuals participated in the study (Table 1).

The diagnosis of cirrhosis was based on histology of liver biopsy specimens in each patient; all patients with

cirrhosis had esophageal varices, indicating portosystemic vascular shunting. The cause was chronic alcoholism in 13 patients, hemochromatosis in 1, and cryptogenic in 1. Precipitating factors for the HE were bleeding from esophageal varices ( $n = 5$ ) and infection ( $n = 3$ ); in no cases were dehydration, diuretic, or other medications considered precipitating factors. All patients with cirrhosis had severely reduced metabolic liver function (Table 1); patients with HE had respiratory alkalosis that was only in part metabolically compensated (Table 1); blood ammonia was increased in patients with cirrhosis, especially in those with HE (Table 1). No patients were treated with branched-chain amino acids, but all HE patients were treated with lactulose. All patients were spontaneously normo-ventilating and hence none was sedated, intubated, or mechanically ventilated.

**Ethics.** The study was performed according to the Helsinki II declaration and approved by the Ethics Committee of Aarhus County. Informed consent was obtained from each subject, except those patients with HE grades III to IV, for whom informed consent was obtained from a next-of-kin. Healthy controls were recruited through an announcement in a local newspaper. The total radioactive dose received by the individuals was, on average, 2.2 mSv. No complications of the procedures occurred in any subject.

**PET Scanning.** Scanning was performed by using a Siemens ECAT EXACT HR PET tomograph (CTI/Siemens, Knoxville, TN). Tracers were produced at the PET center by applying standard techniques and commercially available systems for isotope generation (General Electric, Uppsala, Sweden). The subject was positioned with the brain within the 15-cm field of view of the scanner and the head in a custom-made holder to prevent movements during and between studies. Dynamic emission record-

ings were made after 2 successive intravenous injections of 500 MBq  $^{15}\text{O}$ -water and 2 successive injections of 500 MBq  $^{13}\text{N}$ -ammonia. Eight patients with cirrhosis had only one  $^{13}\text{N}$ -ammonia scan because of technical problems.  $^{15}\text{O}$ -water was administered as a bolus injection over 4 seconds and  $^{13}\text{N}$ -ammonia as a bolus injection over 15 seconds to ensure an adequate number of blood radioactivity measurements in the initial dynamic phase for precise calculation of kinetic parameters.

The dynamic  $^{15}\text{O}$ -water study consisted of 21 time frames:  $10 \times 3$  s,  $3 \times 10$  s, and  $8 \times 15$  s (3 minutes). The  $^{13}\text{N}$ -ammonia study consisted of 27 time frames:  $6 \times 10$  s,  $8 \times 15$  s,  $2 \times 30$  s,  $3 \times 60$  s,  $4 \times 120$  s,  $2 \times 150$  s, and  $2 \times 300$  s (30 minutes). Data were recorded as mean values in each time frame, corrected for attenuation based on an initial 15-minute transmission scan using external Ge 68/64 rotating sources, and corrected for radioactive decay to start of the scanning. Reconstruction was performed by a 2D back-projection algorithm, resulting in 3-dimensional images consisting of  $128 \times 128 \times 47$  voxels of  $2.0 \times 2.0 \times 3.1$  mm<sup>3</sup>. Central spatial resolution was 4.5 mm full-width at half-maximum.

Specific brain regions were identified in images of the mean radioactivity concentrations from the dynamic  $^{13}\text{N}$ -ammonia emission recordings after the first  $^{13}\text{N}$ -ammonia injection (Fig. 1). As seen in Fig. 1, brain regions were quite well defined on this image presentation, and by simultaneous inspection of an average magnetic resonance imaging image based on 7 patients with cirrhosis and 5 healthy controls (Keiding, unpublished data, July 2005), using the Talairach and Tournoux model<sup>27</sup> as a template, regions of interest were drawn in adjacent transaxial slices. The regions of interest were summed to volumes of interest (VOIs) for the right and left frontal cortex, temporal cortex, parietal cortex, occipital cortex, caudate nuclei, thalamus, putamen, and cerebellar lobes. No significant left–right differences were seen in the kinetic parameters within the cortical regions, the basal ganglia, or the cerebellar regions (data not shown). Hence, further analyses were performed for 3 combined VOIs: cortex, basal ganglia, and cerebellum. The VOIs were subsequently placed on images of the mean radioactivity concentrations of the second  $^{13}\text{N}$ -ammonia scan and of the  $^{15}\text{O}$ -water scans. Finally, the VOIs were transferred to the respective dynamic images, and time courses of tissue radioactivity concentrations were extracted (Fig. 2).

**Blood Sampling.** Before scanning, a short catheter (Artflon, Becton Dickinson, Swindon, UK) was placed percutaneously in a radial artery under local anesthesia. During the  $^{15}\text{O}$ -water scans, arterial blood was sampled by an automated blood sampling system<sup>28</sup> cross-calibrated with the tomograph. Radioactivity concentrations

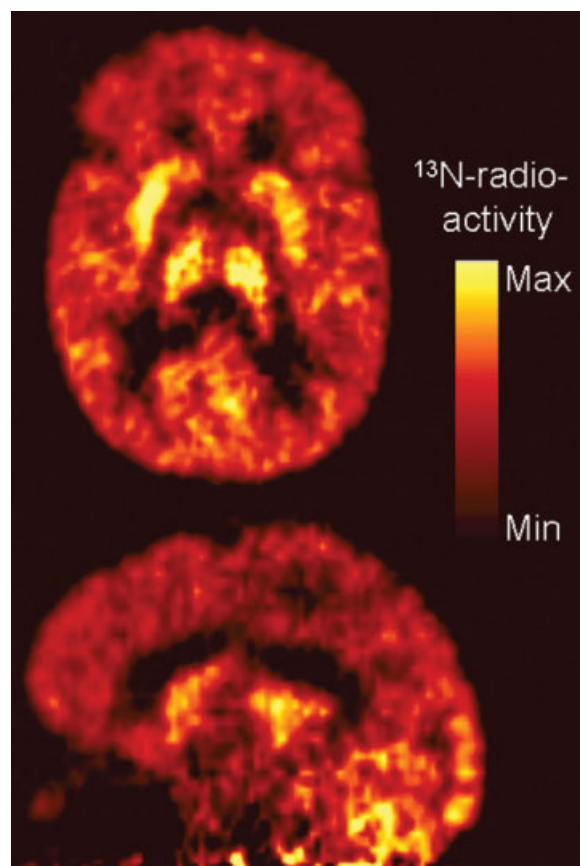


Fig. 1. PET images of transaxial (top) and sagittal (bottom) 3-mm slices showing mean brain  $^{13}\text{N}$ -radioactivity concentrations 0–30 minutes after intravenous injection of 500 MBq  $^{13}\text{N}$ -ammonia in a patient with cirrhosis with an acute episode of HE. PET, positron emission tomography; HE, hepatic encephalopathy.

were measured every 0.5 seconds and corrected for external delay and dispersion in the sampling catheter and for radioactive decay to start of the scan.

During the  $^{13}\text{N}$ -ammonia scans, a series of 24 arterial blood samples of 1 mL each were collected manually at the following intervals:  $12 \times 5$  s,  $3 \times 10$  s,  $1 \times 30$  s,  $1 \times 60$  s,  $2 \times 120$  s,  $1 \times 180$  s, and  $4 \times 300$  s. Total blood  $^{13}\text{N}$ -radioactivity concentrations were measured by using a well counter (Packard Instruments Co., Meriden, CT), cross-calibrated with the tomograph and corrected for radioactive decay to start of the scan.

Additional blood samples were collected at 1, 2, 3, 5, 7, 10, 15, 20, 25, and 30 minutes after the  $^{13}\text{N}$ -ammonia injection for measurements of  $^{13}\text{N}$ -metabolites by solid phase extraction according to Rosenspire et al.,<sup>29</sup> validated by radio–high-pressure liquid chromatography of blood samples at 5 and 15 minutes.<sup>30</sup> Detection of  $^{13}\text{N}$ -ammonia and  $^{13}\text{N}$ -urea were verified by co-injection of  $^{13}\text{N}$ -labeled ammonia and by ultraviolet detection of non-radioactive urea. Based on former studies identifying  $^{13}\text{N}$ -

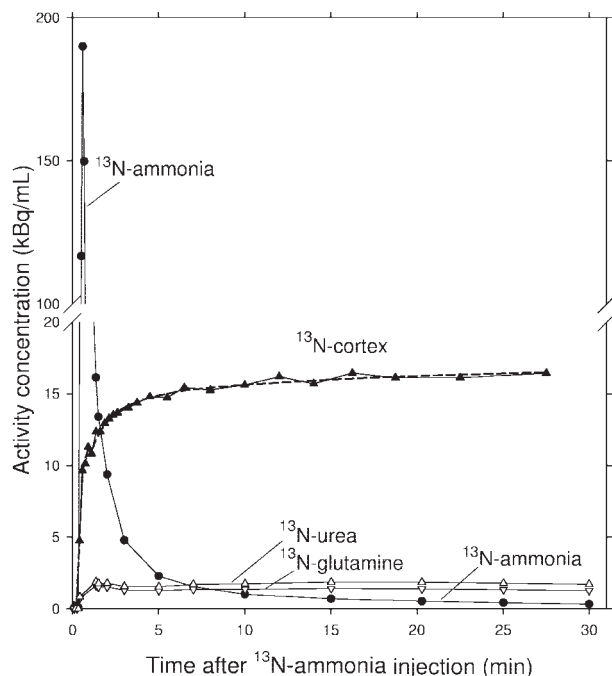


Fig. 2. Time course of  $^{13}\text{N}$ -radioactivity concentrations during 30 minutes in cerebral cortex and arterial blood of  $^{13}\text{N}$ -ammonia,  $^{13}\text{N}$ -urea, and  $^{13}\text{N}$ -glutamine after intravenous injection of 500 MBq  $^{13}\text{N}$ -ammonia in a healthy individual. Measured data points are connected by straight lines. Model fit to the data is shown as a curve.

glutamine by an enzymatic technique, we attributed the single remaining high-pressure liquid chromatography fraction to  $^{13}\text{N}$ -glutamine. Other radiochemical fractions were insignificant or constituted less than 5% of recovered radioactivity. A double-exponential curve was fitted to the time course of the  $^{13}\text{N}$ -ammonia fraction, and mono-exponential curves were fitted to the  $^{13}\text{N}$ -urea and  $^{13}\text{N}$ -glutamine fractions. These fittings were used to estimate continuous individual time-activity curves for  $^{13}\text{N}$ -ammonia,  $^{13}\text{N}$ -urea, and  $^{13}\text{N}$ -glutamine (Fig. 2).

Arterial blood ammonia,<sup>31</sup> pH, standard  $\text{HCO}_3^-$ , and  $\text{pCO}_2$  (ABL, Radiometer, Copenhagen, Denmark) were measured 3 times during the  $^{13}\text{N}$ -ammonia recordings. None of the measurements changed significantly in the course of the scanning period, and mean values were used (Table 1).

**Kinetic Analysis.** Regional cerebral blood flow (CBF) was calculated according to a standard  $^{15}\text{O}$ -water one-tissue compartment model.<sup>32</sup> Clearance of  $^{15}\text{O}$ -water from blood into brain parenchyma,  $K_1$  (mL blood/min/mL tissue), and the rate constant of back-flux from brain parenchyma to blood,  $k_2$  (per minute), were calculated by non-linear fitting of the model to the measured time courses of  $^{15}\text{O}$ -radioactivity concentration in tissue, and using the measured time course of arterial blood  $^{15}\text{O}$ -

radioactivity concentration as input function.<sup>32</sup> Regional CBF (mL blood/min/mL tissue), was calculated as  $\text{CBF} = K_1/0.9$ , where 0.9 corrects for the extraction fraction of  $^{15}\text{O}$ -water in the brain.<sup>33</sup>

The experimental  $^{13}\text{N}$ -ammonia data were analyzed by the two-tissue compartment model of  $^{13}\text{N}$ -ammonia uptake and metabolism illustrated in Fig. 3, characterized by  $^{13}\text{N}$ -ammonia clearance from blood to cell across the BBB,  $K_1$  (mL blood/min/mL tissue), back-flux of  $^{13}\text{N}$ -ammonia by rate constant,  $k_2$  (per minute), and conversion of intracellular  $^{13}\text{N}$ -ammonia to  $^{13}\text{N}$ -glutamine by rate constant,  $k_3$  (per minute).  $^{13}\text{N}$ -urea formed in the liver was assumed to enter and leave brain by diffusion characterized by  $K_1^*$  and  $k_2^*$  equal to kinetic terms for  $^{15}\text{O}$ -water, assuming identical kinetics for the 2 tracers. The kinetic compartment for arterial blood  $^{13}\text{N}$ -ammonia and  $^{13}\text{N}$ -metabolites was fixed at 0.01 mL/mL in accordance with preliminary fitting (data not shown). Kinetic parameters were calculated by non-linear fitting of the model (Fig. 3) to the measured time courses of brain tissue  $^{13}\text{N}$ -radioactivity concentrations, using time courses of blood  $^{13}\text{N}$ -ammonia,  $^{13}\text{N}$ -urea, and  $^{13}\text{N}$ -glutamine as input functions for each subject and each of the 3 brain regions (see Fig. 2).

We use the concept of flow-independent permeability-surface area product ( $PS$ )<sup>34,35</sup> to characterize (1) net transfer of  $^{13}\text{N}$ -ammonia from blood into brain parenchyma across the BBB,  $PS_{\text{BBB}}$  (mL blood/min/mL tissue) and (2) net metabolic conversion of blood  $^{13}\text{N}$ -ammonia into intracellular  $^{13}\text{N}$ -glutamine,  $PS_{\text{met}}$  (mL blood/min/mL tissue):

Kinetic Model of Brain Ammonia Metabolism

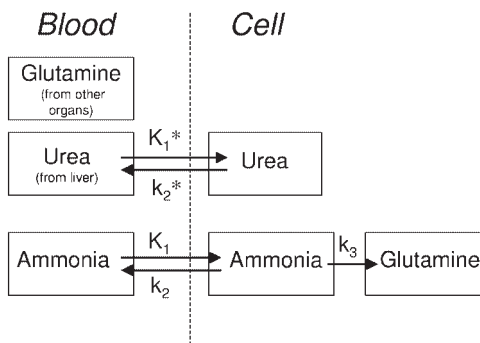


Fig. 3. Compartment model of  $^{13}\text{N}$ -ammonia metabolism in brain:  $^{13}\text{N}$ -ammonia transfer across the blood-brain barrier is characterized by clearance  $K_1$  (mL blood/min/mL tissue) and back-flux rate constant  $k_2$  (per minute).  $^{13}\text{N}$ -urea (formed in the liver) enters and leaves the brain cells characterized by  $K_1^*$  (mL blood/min/mL tissue) and  $k_2^*$  (per minute). Blood  $^{13}\text{N}$ -glutamine is formed in extracerebral tissues (including liver) and distributes in brain vascular volume.

**Table 2. Regional Cerebral Blood Flow and <sup>13</sup>N-Ammonia Kinetic Parameters in Patients With Cirrhosis With and Without an Acute Episode of HE and in Healthy Controls**

		<b>CBF</b> mL blood/ min/mL tissue	<b>K<sub>1</sub></b> mL blood/ min/mL tissue	<b>PS<sub>BBB</sub></b> mL blood/ min/mL tissue	<b>K<sub>met</sub></b> mL blood/ min/mL tissue	<b>PS<sub>met</sub></b> mL blood/ min/mL tissue	<b>Metabolic flux</b> μmol ammonia/ min/L tissue
Cirrhosis with HE (n = 8)	Cortex	0.41 ± 0.04	0.29 ± 0.04	0.21 ± 0.02*	0.15 ± 0.01	0.20 ± 0.01	13.4 ± 0.9**
	Basal ganglia	0.60 ± 0.05	0.36 ± 0.05	0.28 ± 0.03*	0.21 ± 0.01	0.27 ± 0.01	18.2 ± 1.2**
	Cerebellum	0.56 ± 0.06	0.38 ± 0.06	0.20 ± 0.02*	0.19 ± 0.01	0.24 ± 0.01	16.7 ± 1.3**
Cirrhosis without HE (n = 7)	Cortex	0.44 ± 0.03	0.32 ± 0.04	0.31 ± 0.03*	0.20 ± 0.03*	0.23 ± 0.04	7.4 ± 1.4**
	Basal ganglia	0.59 ± 0.04	0.36 ± 0.02	0.37 ± 0.07	0.27 ± 0.04*	0.32 ± 0.04	10.6 ± 2.0**
	Cerebellum	0.58 ± 0.04	0.32 ± 0.03	0.27 ± 0.04	0.24 ± 0.03	0.27 ± 0.03	8.8 ± 1.6**
Healthy controls (n = 5)	Cortex	0.47 ± 0.03	0.29 ± 0.03	0.34 ± 0.03	0.16 ± 0.01	0.20 ± 0.01	2.6 ± 0.3
	Basal ganglia	0.62 ± 0.05	0.31 ± 0.01	0.44 ± 0.03	0.21 ± 0.01	0.26 ± 0.02	3.4 ± 0.3
	Cerebellum	0.64 ± 0.04	0.30 ± 0.02	0.34 ± 0.02	0.19 ± 0.01	0.23 ± 0.01	3.1 ± 0.4

NOTE. Values are given as mean ± standard error of the mean. The \* and \*\* indicate that the mean is statistically significantly different from the corresponding regional value in healthy control group: \**P* < .05; \*\**P* < .01. CBF, cerebral blood flow, is determined from dynamic <sup>15</sup>O-water PET. Dynamic <sup>13</sup>N-ammonia PET estimates: *K*<sub>1</sub>, initial clearance of <sup>13</sup>N-ammonia across blood-brain barrier (BBB) from blood to cells; *PS*<sub>BBB</sub>, blood-brain permeability for <sup>13</sup>N-ammonia; *K*<sub>met</sub>, net metabolic clearance of <sup>13</sup>N-ammonia in blood from intracellular <sup>13</sup>N-metabolites (mainly <sup>13</sup>N-glutamine). *Metabolic flux* of ammonia from blood into brain tissue is calculated as *K*<sub>met</sub> × arterial ammonia concentration.

*PS*<sub>BBB</sub> was calculated according to the Kety-Renkin-Crone relation as

$$PS_{BBB} = -CBF \ln(1 - K_1/CBF) \quad (1)$$

where *K*<sub>1</sub>/*CBF* equals the extraction fraction of the initial distribution of <sup>13</sup>N-ammonia.

Net metabolic clearance of blood <sup>13</sup>N-ammonia into intracellular <sup>13</sup>N-glutamine, *K*<sub>met</sub> (mL blood/min/mL tissue), was calculated as the asymptote of the Gjedde-Patlak linearization<sup>35,36</sup> of the model and equals

$$K_{met} = K_1 k_3 / (k_2 + k_3) \quad (2)$$

*PS*<sub>met</sub> of the metabolic conversion of blood <sup>13</sup>N-ammonia into intracellular <sup>13</sup>N-glutamine was calculated as

$$PS_{met} = -CBF \ln(1 - K_{met}/CBF) \quad (3)$$

where *K*<sub>met</sub>/*CBF* is the extraction fraction of steady state ammonia metabolism.

Metabolic flux of ammonia molecules into glutamine, *Flux*<sub>met</sub> (μmol ammonia/min/L tissue) was calculated as

$$Flux_{met} = K_{met} A \quad (4)$$

where *A* is the arterial blood ammonia concentration (see Table 1).

Correlation between kinetic parameters and their identifiability were examined by sensitivity analysis.<sup>37</sup> This showed that *K*<sub>1</sub> and *PS*<sub>BBB</sub> were mainly determined from the early data when <sup>13</sup>N-ammonia distributes across the BBB, and *K*<sub>met</sub> and *PS*<sub>met</sub> were mainly determined from late data when enzymatic conversion of <sup>13</sup>N-ammonia into <sup>13</sup>N-glutamine dominates the PET signal. Mathematical independence of the kinetic parameters was

shown by the fact that no sensitivity function was proportional to or a reciprocal of another.

**Statistics.** Results are given as mean ± SEM. Calculation of the kinetic parameters from the 3 brain regions in individual subjects were based on the same input curve and thus cannot be assumed to be statistically independent. Accordingly, the Newman-Keuls test was used for comparisons between groups of subjects. In the case of significance, group-wise comparisons of regional parameters were performed by Wilcoxon's test for unpaired data. *P* < .05 was considered statistically significant.

## Results

Duplicate measurements of the regional cerebral blood flow (CBF) in each subject deviated less than 5%, and individual mean values were used for further kinetic calculations. CBF in cortex was on average approximately two thirds of the values in the basal ganglia and cerebellum in each group of subjects and approximately 10% lower in the patients with cirrhosis with HE than in the healthy controls (Table 2).

Duplicate measurements of clearance *K*<sub>1</sub> of the BBB transfer of <sup>13</sup>N-ammonia in 12 subjects deviated less than 13%, and individual mean values were used. There was significant difference neither between cerebral regions nor between groups of subjects (Table 2). The efflux rate constant for ammonia, *k*<sub>2</sub> (mean, approximately 0.1/min) and the rate constant for the glutamine synthetase reaction, *k*<sub>3</sub> (mean, approximately 0.1/min) varied considerably, but all estimates were positive and without systematic differences between groups of individuals or brain regions (data not shown). Efflux of <sup>13</sup>N-glutamine

from brain to blood was not detectable within the current 30-minute study period, as showed by a linear asymptote of the Gjedde-Patlak regression in each case.

For  $PS_{BBB}$ , duplicate determinations in 12 subjects deviated on average 17% (range, 1%-38%), and individual mean values were used. Rank order for mean values was *cirrhosis with HE* < *cirrhosis without HE* < *healthy controls* in each of the 3 brain regions (see Table 2). For each region, values in the group of patients with HE were approximately two thirds of those in the healthy control group (Table 2). There was a tendency to higher values in the basal ganglia than in the other regions in each group of subjects, but the difference did not reach statistical significance.

For  $PS_{met}$  duplicate determinations in 12 subjects deviated on average 6% (range, 1%-24%), and individual mean values were used. Neither significant differences of the metabolic clearance  $K_{met}$  nor of the  $PS_{met}$  between groups of individuals or brain regions were seen, although both values tended to be lower in cerebral cortex than in the other regions (see Table 2).

Flux of non-radioactive blood ammonia into intracellular glutamine,  $Flux_{met}$  (equation 4) showed no significant regional variations, although the rank order was *cortex* < *cerebellum* < *basal ganglia* within each groups of subjects (Table 2). Mean values were remarkably higher in the 2 cirrhotic groups with cirrhosis than in the healthy control group, especially in the HE group (Table 2). Figure 4 shows a linear relation between ammonia flux and endogenous blood ammonia for each of the 3 brain regions. The slope for the cortex relation tended to be lower than that for the 2 other regions in accordance with the tendency for lower cortical  $K_{met}$  values.

## Discussion

Brain ammonia metabolism constitutes 2 successive steps: (1) transfer across the BBB and (2) enzymatic conversion into glutamine in the astrocyte (Fig. 3). The permeability–surface area product  $PS_{BBB}$  characterizes transfer of ammonia from blood to brain parenchyma across the BBB. There may be intracellular and extracellular compartments within the brain, but in the modeling they are united into a single tissue compartment.  $PS_{BBB}$  was reduced in each of the 3 brain regions in patients with cirrhosis, especially in those with HE, compared with healthy controls (Table 2). The physiological parameter  $PS_{met}$  characterizes the combined transfer of ammonia from blood to brain parenchyma and the subsequent enzymatic conversion to glutamine; it was not significantly different between the 3 groups of individuals. As is discussed later, these results are in contrast to prevailing views that  $PS$ -values for  $^{13}\text{N}$ -ammonia are increased in

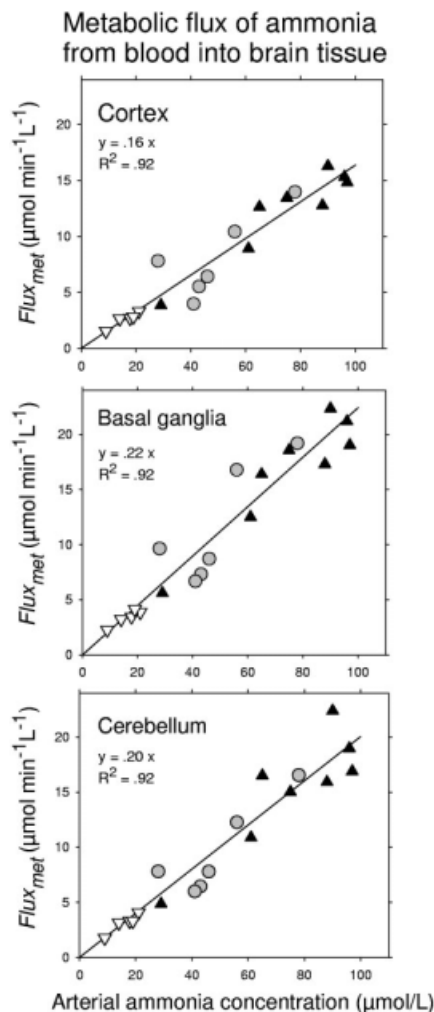


Fig. 4. Metabolic flux ammonia from blood into intracellular glutamine,  $Flux_{met}$ , in relation to arterial blood ammonia for cerebral regions as indicated for patients with cirrhosis with HE (closed triangle), patients with cirrhosis without HE (circle), and healthy controls (open triangle). Straight lines show linear regressions through 0.0 with the slopes (i.e., average  $K_{met}$ ) indicated. HE, hepatic encephalopathy.

HE.<sup>4,20-22</sup> Current methods, however, constitute a significant improvement through the use of the improved spatial and temporal resolution of contemporary PET technology, the use of selective measurements of labeled ammonia and its metabolites in blood to characterize the input function, and the application of physiological modeling for examination of complex metabolic processes *in vivo*.

The compartment model of  $^{13}\text{N}$ -ammonia distribution and metabolism illustrated in Fig. 3 is a simplified depiction of the true complexity of brain ammonia metabolism.<sup>4</sup> This simplification is required by the inability of PET recordings to distinguish multiple metabolic compartments in the brain. We first explored a model that ignored blood–brain transfer of  $^{13}\text{N}$ -urea and cerebral distribution of  $^{13}\text{N}$ -glutamine and used only blood  $^{13}\text{N}$ -

ammonia as the input; however, fitting of this model to the PET data was clearly biased. Separate accounting for blood  $^{13}\text{N}$ -metabolites improved the goodness of fitting considerably as evaluated by residuals of the fitting and the Akaike score.<sup>38</sup> This finding is probably related to the rapid depletion of  $^{13}\text{N}$ -ammonia in blood and rapid  $^{13}\text{N}$ -metabolite formation (Fig. 2).

The variable, but positive  $k_2$  estimate in each brain region is consistent with a minor back-flux of  $^{13}\text{N}$ -ammonia, as must be the case for simple diffusion across the BBB.<sup>4,39,40</sup> The rate constant for the glutamine synthetase reaction,  $k_3$ , similarly varied but was positive in each case, and tended to be higher in the HE group than in the other groups. There was no detectable efflux of  $^{13}\text{N}$ -glutamine from brain to blood within the current 30-minute study period, which is in agreement with previous observations.<sup>5,41,42</sup> Accordingly, brain  $^{13}\text{N}$ -concentration (Fig. 2) may be ascribed initially to passage of the blood tracer bolus and blood-to-brain transfer of  $^{13}\text{N}$ -ammonia and after the first few minutes to accumulation of  $^{13}\text{N}$ -glutamine, in agreement with findings in  $^{13}\text{N}$ -ammonia PET pig liver studies.<sup>43</sup>

There was a tendency to lower cerebral blood flow rates in the cirrhosis groups than in the control group (Table 2) in each of the 3 regions, but this did not reach statistical significance. Studies have shown CBF to reduce with aging<sup>44</sup> and the current findings may be related to the somewhat higher mean age of the cirrhosis groups than that of the control group (Table 1). Regional variations similar to the current findings were found in 2 other  $^{15}\text{O}$ -water PET studies of healthy controls and patients with minimal HE.<sup>23,45</sup> The reasons for the variations are not known but may be related to variations in the distribution of carbohydrate<sup>45</sup> and ammonia metabolism.<sup>20,23</sup>

The reduction of the BBB permeability  $PS_{BBB}$  for  $^{13}\text{N}$ -ammonia in HE patients to approximately two thirds of control values in cerebral cortex, basal ganglia, and cerebellum is a novel finding of the current study. Mean cortex  $PS_{BBB}$  in the 4 patients with HE grades III to IV was 0.15 mL/min/mL tissue and that in patients with HE grades I to II 0.26 mL/min/mL tissue. No earlier study has reported measurements of BBB ammonia transfer in patients with cirrhosis with clinically overt HE, and the current results indicate that the more severe the HE grade, the lower the  $PS_{BBB}$ . Ahl et al.<sup>23</sup> found no significant differences of  $PS_{BBB}$  of  $^{13}\text{N}$ -ammonia in 5 patients with cirrhosis with minimal HE and 3 patients with cirrhosis without HE; the average was 0.24 mL/min/mL tissue. The magnitude of this estimate is lower than in the current patients with cirrhosis without HE, approximately 0.31 mL/min/mL tissue (Table 2). However, we used individually measured corrections of  $^{13}\text{N}$ -metabolites in

the input whereas Ahl et al.<sup>23</sup> used a common  $^{13}\text{N}$ -metabolite correction taken from a separate study of healthy controls,<sup>29</sup> a methodological difference that most likely explains the discrepancy between the results of the 2 studies. Regional variations, with a tendency to higher  $PS_{BBB}$  values in the basal ganglia (Table 2), were found in both studies.

Transfer of ammonia across the BBB is generally thought to be mediated by simple diffusion of  $\text{NH}_3$  and specific  $\text{NH}_4^+$  transport proteins.<sup>4</sup> In that case, the slight alkalosis seen in our patients might tend to favor the  $\text{NH}_3$  transfer and thus increase the  $PS_{BBB}$ . However, the opposite was actually observed, indicating that a pH effect cannot explain our findings. The reduced  $PS_{BBB}$  in the patients with cirrhosis with HE might be linked to inflammatory factors<sup>46</sup> or increased diffusion distance through an increased extracellular volume in patients with cirrhosis with low-grade cerebral edema.<sup>47</sup> It also could be related to other abnormalities such as altered membrane properties attributable to long-term exposure to elevated blood ammonia in analogy with the decreased membrane fluidity observed in patients with chronic high alcohol intake.<sup>48</sup> Finally, the activity of specific transport proteins for  $\text{NH}_4^+$  in the BBB<sup>4</sup> may be altered because of high ammonia concentrations.

The  $PS_{met}$ , the permeability–surface product of the metabolic conversion of blood  $^{13}\text{N}$ -ammonia into intracellular  $^{13}\text{N}$ -glutamine, tended to be higher in the basal ganglia than in the 2 other brain regions, but the difference did not reach statistical significance (Table 2). Distinguishing between kinetic parameters of the BBB (permeability  $PS_{BBB}$  related to initial transfer of ammonia across the BBB) and metabolism ( $PS_{met}$  related to steady-state metabolic conversion of ammonia to glutamine in the cells) is important. Lockwood et al.,<sup>20–22</sup> in 1979 published pioneer work of brain ammonia metabolism using  $^{13}\text{N}$ -ammonia scans and in 1984 and 1991 estimated a  $PS$  value that corresponds to  $PS_{met}$ : they multiplied the amount of tracer in the brain (static PET of the brain in the interval 10 to 25 minutes after tracer injection) relative to the amount of tracer in the body (scan from head to upper leg) with a clearance value estimated from the first 10 minutes after tracer injection of arterial time course of non-metabolized ammonia. Thus, they calculated the fraction of the total body clearance that on average was retained in the brain during the scan and then calculated a  $PS$  value according to equation 3. They did not use initial PET recordings within the very first minutes after tracer injection and thus did not estimate initial kinetic parameters such as  $PS_{BBB}$  as in the current work and in that of Ahl et al.<sup>23</sup> The current dynamic scanning sequences in conjunction with compartmental analysis use

the better temporal and spatial resolution of contemporary PET technology and also specified the separate inputs of blood  $^{13}\text{N}$ -ammonia and  $^{13}\text{N}$ -metabolites, thus yielding results based on a superior physiological model. We therefore conclude that regional  $PS_{met}$  is not changed significantly in patients with cirrhosis with or without HE compared with healthy controls (Table 2).

The finding of increased flux of blood ammonia into intracellular glutamine,  $Flux_{met}$  (Table 2 and Fig. 4), in patients with cirrhosis compared with healthy controls is similar to that found by Lockwood et al.<sup>20</sup> The magnitude of  $Flux_{met}$  was significantly correlated to blood ammonia (Fig. 4). The regional differences (Fig. 4) indicate that the basal ganglia and cerebellum might be more sensitive than cortex to changes in blood ammonia.

In conclusion, contemporary dynamic PET technique showed decreased BBB permeability for ammonia,  $PS_{BBB}$ , in patients with cirrhosis with HE to approximately two thirds of control values. Secondly,  $PS_{met}$  of the cerebral metabolic trapping of ammonia as glutamine was unchanged in patients with cirrhosis, whereas the flux of blood ammonia into brain tissue was markedly increased in both patients with cirrhosis with and without HE, depending primarily on arterial blood ammonia. Thus, elevated blood ammonia in cirrhosis rather than changed ammonia kinetics determines brain uptake and possible neurotoxic effects of ammonia.

*Acknowledgment:* The authors thank Paul Cumming for pivotal reading of the manuscript.

## References

1. Sherlock S, Summerskill WH, White LP, Phear EA. Portal-systemic encephalopathy; neurological complications of liver disease. *Lancet* 1954; 267:454-457.
2. Cooper AJ, Plum F. Biochemistry and physiology of brain ammonia. *Physiol Rev* 1987;67:440-519.
3. Butterworth RF. Pathophysiology of hepatic encephalopathy: a new look at ammonia. *Metab Brain Dis* 2002;17:221-227.
4. Ott P, Larsen FS. Blood-brain barrier permeability to ammonia in liver failure: a critical reappraisal. *Neurochem Int* 2004;44:185-198.
5. Gjedde A, Lockwood AH, Duffy TE, Plum F. Cerebral blood flow and metabolism in chronically hyperammonemic rats: effect of an acute ammonia challenge. *Ann Neurol* 1978;3:325-330.
6. Mans AM, Biebuyck JF, Davis DW, Hawkins RA. Portacaval anastomosis: brain and plasma metabolite abnormalities and the effect of nutritional therapy. *J Neurochem* 1984;43:697-705.
7. Rigotti P, Jonung T, Peters JC, James JH, Fischer JE. Methionine sulfoximine prevents the accumulation of large neutral amino acids in brain of portacaval-shunted rats. *J Neurochem* 1985;44:929-933.
8. Butterworth RF, Girard G, Giguere JF. Regional differences in the capacity for ammonia removal by brain following portacaval anastomosis. *J Neurochem* 1988;51:486-490.
9. Girard G, Giguere JF, Butterworth RF. Region-selective reductions in activities of glutamine synthetase in rat brain following portacaval anastomosis. *Metab Brain Dis* 1993;8:207-215.
10. Hawkins RA, Jessy J, Mans AM, De Joseph MR. Effect of reducing brain glutamine synthesis on metabolic symptoms of hepatic encephalopathy. *J Neurochem* 1993;60:1000-1006.
11. Desjardins P, Rao KV, Michalak A, Rose C, Butterworth RF. Effect of portacaval anastomosis on glutamine synthetase protein and gene expression in brain, liver and skeletal muscle. *Metab Brain Dis* 1999;14:273-280.
12. Cooper AJ, Mora SN, Cruz NF, Gelbard AS. Cerebral ammonia metabolism in hyperammonemic rats. *J Neurochem* 1985;44:1716-1723.
13. Hawkins RA, Jessy J. Hyperammonaemia does not impair brain function in the absence of net glutamine synthesis. *Biochem J* 1991;277:697-703.
14. Norenberg MD. Astroglial dysfunction in hepatic encephalopathy. *Metab Brain Dis* 1998;13:319-335.
15. Lavoie J, Giguere J-F, Layrargues GP, Butterworth RF. Amino acid changes in autopsied brain tissue from cirrhotic patients with hepatic encephalopathy. *J Neurochem* 1987;49:692-697.
16. Bessman SP, Bessmann AN. The cerebral and peripheral uptake of ammonia in liver disease with an hypothesis for the mechanism of hepatic coma. *J Clin Invest* 1955;34:622-628.
17. Eriksson LS, Law DH, Hagenfeldt L, Wahren J. Nitrogen metabolism of the human brain. *J Neurochem* 1983;41:1324-1328.
18. Strauss GI, Knudsen GM, Kondrup J, Moller K, Larsen FS. Cerebral metabolism of ammonia and amino acids in patients with fulminant hepatic failure. *Gastroenterology* 2001;121:1109-1119.
19. Phelps ME, Hoffman EJ, Coleman RE, Welch MJ, Raichle ME, Weiss ES, et al. Tomographic images of blood pool and perfusion in brain and heart. *J Nucl Med* 1976;17:603-612.
20. Lockwood AH, McDonald JM, Reiman RE, Gelbard AS, Laughlin JS, Duffy TE, et al. The dynamics of ammonia metabolism in man. Effects of liver disease and hyperammonemia. *J Clin Invest* 1979;63:449-460.
21. Lockwood AH, Bolomey L, Napoleon F. Blood-brain barrier to ammonia in humans. *J Cereb Blood Flow Metab* 1984;4:516-522.
22. Lockwood AH, Yap EW, Wong WH. Cerebral ammonia metabolism in patients with severe liver disease and minimal hepatic encephalopathy. *J Cereb Blood Flow Metab* 1991;11:337-341.
23. Ahl B, Weissenborn K, van den Hoff J, Fischer-Wasels D, Köstler H, Hecker H, et al. Regional differences in cerebral blood flow and cerebral ammonia metabolism in patients with cirrhosis. *HEPATOLOGY* 2004;40: 73-79.
24. Conn HO, Lieberthal MM. *The Hepatic Coma Syndromes and Lactulose*. Baltimore: Williams & Williams, 1979.
25. Ferenci P, Lockwood A, Mullen K, Tarter R, Weissenborn K, Blei AT. Hepatic encephalopathy—definition, nomenclature, diagnosis, and quantification: final report of the working party at the 11th World Congresses of Gastroenterology, Vienna, 1998. *HEPATOLOGY* 2002;35:716-721.
26. Teasdale G, Knill-Jones R, van der Sande J. Observer variability in assessing impaired consciousness and coma. *J Neurol Neurosurg Psychiatry*. 1978;41:603-610.
27. Talairach J, Tournoux P. *Co-planar stereotaxic Atlas of the Human Brain*. 2nd ed. Stuttgart: Thieme Verlag, 1998.
28. Vafae M, Murase K, Gjedde A, Meyer E. Dispersion correction for automatic sampling of O-15 labeled H2O and red blood cells. In: Meyers R, Cunningham V, Bailey D, Jones T, eds. *Quantification of Brain Function Using PET*. San Diego, CA: Academic Press, 1996:72-75.
29. Rosenspire KC, Schwaiger M, Mangner TJ, Hutchins GD, Sutorik A, Kuhl DE. Metabolic fate of [ $^{13}\text{N}$ ]ammonia in human and canine blood. *J Nucl Med* 1990;31:163-167.
30. Nieves E, Rosenspire KC, Filic-DeRico S, Gelbard AS, Cooper AJ. High-performance liquid chromatographic on-line flow-through radioactivity detector system for analyzing amino acids and metabolites labeled with nitrogen-13. *J Chromatogr* 1986;383:325-337.
31. van Anken HC, Schiphorst ME. A kinetic determination of ammonia in plasma. *Clin Chim Acta* 1974;56:151-157.
32. Ohta S, Meyer E, Fujita H, Reutens DC, Evans A, Gjedde A. Cerebral [ $^{15}\text{O}$ ]water clearance in humans determined by PET: I. Theory and normal values. *J Cereb Blood Flow Metab* 1996;16:765-780.

33. Raichle ME, Martin WR, Herscovitch P, Mintun MA, Markham J. Brain blood flow measured with intravenous  $H_2^{15}O$ . II. Implementation and validation. *J Nucl Med* 1983;24:790-798.
34. Keiding S. Dynamic aspects of hepatic removal of circulating substances. In: McIntyre N, Benhamou J-P, Bircher J, Rizzetto M, Rodes J, eds. *Oxford Textbook of Clinical Hepatology*. Oxford University Press 1991: 78-87.
35. Gjedde A. Calculation of cerebral glucose phosphorylation from brain uptake of glucose analogs in vivo: a re-examination. *Brain Res*. 1982;257: 237-274.
36. Patlak CS, Blasberg RG, Fenstermacher JD. Graphical evaluation of blood-to-brain transfer constants from multiple-time uptake data. *J Cereb Blood Flow Metab* 1983;3:1-7.
37. Munk OL, Bass L, Roelsgaard K, Bender D, Hansen SB, Keiding S. Liver kinetics of glucose analogs measured in pigs by PET: importance of dual-input blood sampling. *J Nucl Med* 2001;42:795-801.
38. Akaike H. A new look at the statistical model identification. *IEEE Trans Automat Control* 1974;19:716-723.
39. Phelps ME, Huang SC, Hoffman EJ, Selin C, Kuhl DE. Cerebral extraction of N-13 ammonia: its dependence on cerebral blood flow and capillary permeability - surface area product. *Stroke* 1981;12:607-619.
40. Raichle ME, Larson KB. The significance of the  $NH_3-NH_4^+$  equilibrium on the passage of  $^{13}N$ -ammonia from blood to brain: a new regional residue detection model. *Circ Res* 1981;48:913-937.
41. James JH, Fischer JE. Transport of neutral amino acids at the blood-brain barrier. *Pharmacology* 1981;22:1-7.
42. Oldendorf WH, Szabo J. Amino acid assignment to one of three blood-brain barrier amino acid carriers. *Am J Physiol* 1976;230:94-98.
43. Keiding S, Munk O, Roelsgaard K, Bender D, Bass L. Positron emission tomography of hepatic first-pass metabolism of ammonia in pig. *Eur J Nucl Med Mol Imaging* 2001;28:1770-1775.
44. Marchal G, Rioux P, Petit-Taboue MC, Sette G, Traverso JM, Le Poec C, et al. Regional cerebral oxygen consumption, blood flow, and blood volume in healthy human aging. *Arch Neurol* 1992;49:1013-1020.
45. Lockwood AH, Yap EW, Rhoades HM, Wong WH. Altered cerebral blood flow and glucose metabolism in patients with liver disease and minimal encephalopathy. *J Cereb Blood Flow Metab* 1991;11:331-336.
46. Blei A. Infection, inflammation and hepatic encephalopathy, synergism redefined. *J Hepatol* 2004;40:327-330.
47. Häussinger D, Kircheis G, Fischer R, Schliess F, vom Dahl S. Hepatic encephalopathy in chronic liver disease: a clinical manifestation of astrocyte swelling and low-grade cerebral edema? *J Hepatol* 2000;32:1035-1038.
48. Stibler H, Beauge F, Leguicher A, Borg S. Biophysical and biochemical alterations in erythrocyte membranes from chronic alcoholics. *Scand J Clin Lab Invest* 1991;51:309-319.
49. Tygstrup N. Determination of the hepatic galactose elimination capacity after a single intravenous injection in man: the reproducibility and the influence of uneven distribution. *Acta Physiol Scand* 1963;58:162-172.
50. Pugh RN, Murray-Lyon IM, Dawson JL, Pietroni MC, Williams R. Transection of the oesophagus for bleeding oesophageal varices. *Br J Surg* 1973; 60:646-649.

## Hepatology 2006; 44:1056. ERRATUM

In the article entitled "Brain Metabolism of  $^{13}\text{N}$ -Ammonia During Acute Hepatic Encephalopathy in Cirrhosis Measured by Positron Emission Tomography" by Keiding et al. (HEPATOLOGY 2006;43:42-50), there was an arithmetical error in the calculations of  $PS_{BBB}$  in Table 2. The Table below gives corrected values. Since the  $PS_{BBB}$  calculation is based on individual values of cerebral blood flow,  $CBF$ , and the initial unidirectional clearance of  $^{13}\text{N}$ -ammonia,  $K_I$ , as  $PS_{BBB} = -CBF \ln(1-K_I/CBF)$ , mean values of  $CBF$  and  $K_I$  now include only individuals where both  $CBF$  and  $K_I$  were measured. Mean  $PS_{BBB}$  values in the group of patients with cirrhosis and HE were lower than mean values in the group of healthy controls but the difference was not statistically significant.

**Table 2. Regional Cerebral Blood Flow and  $^{13}\text{N}$ -Ammonia Kinetic Parameters in Cirrhotic Patients With and Without an Acute Episode of HE and in Healthy Controls**

		<i>CBF</i> mL blood/ min/mL tissue	<i>K<sub>I</sub></i> mL blood/ min/mL tissue	<i>PS<sub>BBB</sub></i> mL blood/ min/mL tissue	<i>K<sub>met</sub></i> mL blood/ min/mL tissue	<i>PS<sub>met</sub></i> mL blood/ min mL tissue	<i>Metabolic flux</i> μmol ammonia/ min/L tissue
Cirrhosis with HE (n)	<b>Cortex</b>	0.38±0.03	0.23±0.01	0.37±0.03	0.15±0.01	0.20±0.01	13.4±0.9**
	<b>Basal ganglia</b>	0.56±0.04	0.31±0.02	0.43±0.03	0.21±0.01	0.27±0.01	18.2±1.2**
	<b>Cerebellum</b>	0.52±0.05	0.26±0.02	0.37±0.02	0.19±0.01	0.24±0.01	16.7±1.3**
		6	6	6	8	8	8
Cirrhosis without HE (n)	<b>Cortex</b>	0.44±0.06	0.26±0.02	0.42±0.07	0.20±0.03*	0.23±0.04	7.4±1.4**
	<b>Basal ganglia</b>	0.59±0.05	0.36±0.02	0.59±0.07	0.27±0.04*	0.32±0.04	10.6±2.0**
	<b>Cerebellum</b>	0.59±0.07	0.30±0.03	0.44±0.07	0.24±0.03	0.27±0.03	8.8±1.6**
		5	5	5	7	7	7
Healthy Controls (n)	<b>Cortex</b>	0.47±0.03	0.29±0.03	0.46±0.08	0.16±0.01	0.20±0.01	2.6±0.3
	<b>Basal ganglia</b>	0.62±0.05	0.31±0.01	0.45±0.02	0.21±0.01	0.26±0.02	3.4±0.3
	<b>Cerebellum</b>	0.64±0.04	0.30±0.02	0.41±0.04	0.19±0.01	0.23±0.01	3.1±0.4
		5	5	5	5	5	5

NOTE. Values are given as mean ± standard error of the mean; n, number of subjects. The \* and \*\* indicate that the mean is statistically significantly different from the corresponding regional value in healthy control group: \*)  $P < .05$ ; \*\*)  $P < .01$ . *CBF*, cerebral blood flow, was determined from dynamic  $^{15}\text{O}$ -water PET. Dynamic  $^{13}\text{N}$ -ammonia PET estimates: *K<sub>I</sub>*, initial clearance of  $^{13}\text{N}$ -ammonia across blood-brain barrier (BBB) from blood to cells; *PS<sub>BBB</sub>*, blood-brain permeability for  $^{13}\text{N}$ -ammonia; *K<sub>met</sub>*, net metabolic clearance of  $^{13}\text{N}$ -ammonia in blood to intracellular  $^{13}\text{N}$ -metabolites (mainly  $^{13}\text{N}$ -glutamine). *Metabolic flux* of ammonia from blood into brain tissue was calculated as *K<sub>met</sub>* multiplied by arterial ammonia concentration.